CHEMISTRY
A EUROPEAN JOURNAL

DOI: 10.1002/chem.200700128

Rational Synthetic Tuning between Itinerant Antiferromagnetism and Ferromagnetism in the Complex Boride Series $Sc_2FeRu_{5-n}Rh_nB_2$ ($0 \leq n \leq 5$)

Boniface P. T. Fokwa,* Heiko Lueken, and Richard Dronskowski[a]

Abstract: Single crystals of the complex boride series $Sc_2FeRu_{5-n}Rh_nB_2$ ($n=1$, 3, 4) were synthesized by arc-melting the elements in water-cooled copper crucibles under argon atmospheres and were chemically characterized by single-crystal XRD and EDX analyses. The new compounds are isotypic and crystallize in the tetragonal space group $P4/mbm$ with $Z=2$, adopting a substitutional variant of the $Ti_3Co_5B_2$-type structure. The magnetically active iron atoms are arranged in chains with intra- and interchain distances of about 3.02 and 6.60 Å, respectively. Strong ferromagnetic interactions are observed for both $Sc_2FeRuRh_4B_2$ (64 valence electrons (VE), $T_C \approx 350$ K, $\mu_a = 3.1\ \mu_B$) and $Sc_2FeRu_2Rh_3B_2$ (63 VE, $T_C \approx 300$ K, $\mu_a = 3.0\ \mu_B$), whereas antiferromagnetic interactions are found in the case of $Sc_2FeRu_4RhB_2$ (61 VE, $T_N \approx 10$ K, $\mu_{eff} = 3.2$): The magnetism of the entire $Sc_2FeRu_{5-n}Rh_nB_2$ ($0 \leq n \leq 5$) series is discussed based on the variable valence-electron count and the resulting Fe–Fe bonding character, and it is also compared with other isoelectronic systems.

Keywords: antiferromagnetism · ferromagnetism · intermetallic phases · solid-state structures · valence-electron count

Introduction

The search for novel (intermetallic) materials with both unique crystal structures and extraordinary physical properties is an ongoing challenge for solid-state chemists. Within the last decade, ordered substitutional variants of the $Ti_3Co_5B_2$-type structure[1] with the general composition $A_2MM'_5B_2$ (A: Mg, Sc; M: Mn, Fe, Co, Ni; M′: Ru, Rh, Ir) have been intensively investigated both experimentally and theoretically, in particular with respect to itinerant magnetism.[2–5] These phases exhibit a truly outstanding structural unit, namely well-separated chains of magnetic 3d atoms (M) with intrachain and interchain distances of about 3.0 and 6.6 Å, respectively. Studies of magnetic properties have yielded evidence for both antiferromagnetic (e.g., $Mg_2MnRh_5B_2$) and ferromagnetic materials (e.g., $Sc_2FeRh_5B_2$ with $T_C = 450$ K).

A simple, but rather general classification of potential antiferromagnets and ferromagnets rooted in bond-theoretical ideas[6] was then applied for these compounds.[5] As evidenced from non-spin-polarized Crystal Orbital Hamilton Population (COHP) analyses, phases with 62 valence electrons (VE) exhibit nonbonding M–M states at the Fermi level, thereby suggesting antiferromagnetic behavior, for example, as seen for $Mg_2MnRh_5B_2$ (62 VE: 2×2 for Mg, 1×7 for Mn, 5×9 for Rh, and 2×3 for B). Whenever antibonding M–M states appear at the Fermi level, such as, for 65 VE, the intermetallic phases should show ferromagnetic behavior (e.g., $Sc_2FeRh_5B_2$). Nothing can be safely predicted, however, below the 62 VE limit and for the 62–65 VE regime, and therefore, these questions require further experimental investigations which is the intention of this work.

To do so, the series of compounds $Sc_2FeRu_{5-n}Rh_nB_2$ ($0 \leq n \leq 5$) allows for a synthetic scan of adequate candidates for the investigation of the range $60 \leq VE \leq 65$, in particular given the fact that they differ from each other exclusively in the Ru/Rh ratio, and thus, they seem ideal for the chemical tuning of the VE. The representatives of this series with $n=$ 0, 2, and 5 are already known; as a consequence, we may concentrate on the remaining members of the series with $n=1$, 3, and 4. These phases will be structurally and magnetically described and also grouped in view of their places in the complete series. Moreover, the results will be compared with those compounds having the same nominal VE number, but a different chemical composition.

[a] Dr. B. P. T. Fokwa, Prof. Dr. H. Lueken, Prof. Dr. R. Dronskowski
Institute of Inorganic Chemistry
RWTH Aachen University
52056 Aachen (Germany)
Fax: (+49) 241-80-92642
E-mail: boniface.fokwa@ac.rwth-aachen.de

WILEY InterScience DISCOVER SOMETHING GREAT
© 2007 Wiley-VCH Verlag GmbH & Co. KGaA, Weinheim

Results and Discussion

Crystal chemistry

The obtained powder X-ray diffractograms for $Sc_2FeRu_4RhB_2$, $Sc_2FeRu_2Rh_3B_2$, and $Sc_2FeRuRh_4B_2$ showed a single phase, and the refinement of the unit-cell parameters led to values given in Table 1; in order to obtain higher precision, the powder lattice parameters were also used for the refinement of the single crystal data. All three compounds are isotypic and crystallize as substitutional variants of the $Ti_3Co_5B_2$-type structure. No superstructure lines were observed, thus rhodium and ruthenium atoms must be randomly distributed at their sites. A perspective view of the structure along [001] is shown in the upper part of Figure 1. The structure contains trigonal, tetragonal, and pentagonal prisms of the M′ atoms (M′: Ru and Rh, sharing the same site, but with different ratios, see Table 2) stacked on top of each other, thereby building channels along the [001] direction (Figure 1, top). Because the trigonal prisms are centered by boron atoms, the pentagonal prisms accommodate the scandium atoms and the tetragonal prisms contain the magnetically active iron atoms. The iron and scandium atoms are arranged in chains with the same intrachain distance of about

Table 1. Crystallographic data for $Sc_2FeRu_4RhB_2$, $Sc_2FeRu_2Rh_3B_2$, and $Sc_2FeRuRh_4B_2$.

formula	$Sc_2FeRu_4RhB_2$	$Sc_2FeRu_2Rh_3B_2$	$Sc_2FeRuRh_4B_2$
F_w [g mol^{-1}]	674.6	678.3	680.1
F(000)	598	602	604
crystal size [mm^3]	0.10×0.08×0.06	0.18×0.04×0.03	0.25×0.08×0.08
T [K]		273 (2)	
$2\theta_{max}$ [°]	72.1	71.4	71.4
no. refls; R_{int}	4383; 0.0182	4404; 0.0511	4402; 0.0189
no. indep refls	374	367	370
no. parameters	19	19	19
space group; Z		*P*4/*mbm* (no. 127); 2	
cell parameters			
a [Å]	9.3225(14)	9.3489(15)	9.3491(17)
c [Å]	3.0117(5)	3.0192(6)	3.0187(6)
V [Å^3]	261.74(7)	263.88(8)	263.85(9)
ρ_{calcd} [g cm^{-3}]	8.56	8.54	8.56
μ [mm^{-1}]	19.24	19.61	19.88
absorption correction		semiempirical	
min; max transmission	0.173; 0.314	0.408; 0.556	0.154; 0.206
extinction parameter	0.022(2)	0.010(2)	0.013(2)
diff. peak; hole [e Å^{-3}]	1.15; −1.37	1.58; −3.18	1.65; −3.16
R_1 (all I)	0.0260	0.0410	0.0297

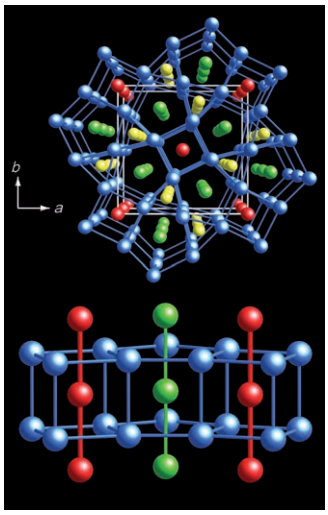

Figure 1. Perspective view of the crystal structure of the compound series $Sc_2FeRu_{5-n}Rh_nB_2$ along the [001] direction (top) and of a part of the structure showing the intrachain (≈3.02 Å) and interchain (≈6.60 Å) Fe–Fe interactions (bottom): ● represent Sc atoms, ● represent Fe atoms, ● represent Ru/Rh atoms, and ● represent B atoms.

Table 2. Atomic coordinates and displacement parameters (10^{-4} Å^2) for $Sc_2FeRu_4RhB_2$, $Sc_2FeRu_2Rh_3B_2$, and $Sc_2FeRuRh_4B_2$. M′ replaces the atoms Ru and Rh sharing the same site (M′1 = Ru1/Rh1, M′2 = Ru2/Rh2).

Atom	x	y	z	Occupancy	U_{eq}[a]	U_{11}	U_{22}	U_{33}	U_{12}
				$Sc_2FeRu_4RhB_2$					
Sc	0.1746(1)	0.6747 (1)	0	1.0	78(2)	85(3)	85(3)	63(5)	−35(4)
Fe	0	0	0	1.0	79(3)	61(4)	61(4)	116(6)	0
M′1	0.0713(1)	0.2147(1)	1/2	Ru1:0.8 Rh1:0.2	72(2)	60(2)	53(2)	102(2)	4(2)
M′2	0	1/2	1/2	Ru2:0.8 Rh2:0.2	52(2)	45(2)	45(2)	66(3)	7(2)
B	0.6240(6)	0.1240(6)	0	1.0	9(2)	–	–	–	–
				$Sc_2FeRu_2Rh_3B_2$					
Sc	0.1750(1)	0.6750 (1)	0	1.0	75(3)	88(5)	88(5)	51(7)	−23(6)
Fe	0	0	0	1.0	132(5)	122(7)	122(7)	151(9)	0
M′1	0.0708(1)	0.2150(1)	1/2	Ru1:0.4 Rh1:0.6	61(2)	65(3)	53(3)	63(3)	−2(2)
M′2	0	1/2	1/2	Ru2:0.4 Rh2:0.6	56(2)	55(3)	55(3)	58(5)	−5(3)
B	0.6251(10)	0.1251(10)	0	1.0	11(2)	–	–	–	–
				$Sc_2FeRuRh_4B_2$					
Sc	0.1752(2)	0.6752 (2)	0	1.0	70(3)	78(4)	78(4)	54(6)	−27(5)
Fe	0	0	0	1.0	97(4)	93(5)	93(5)	111(8)	0
M′1	0.0708(1)	0.2167(1)	1/2	Ru1:0.2 Rh1:0.8	61(2)	60(2)	50(2)	72(3)	−1(1)
M′2	0	1/2	1/2	Ru2:0.2 Rh2:0.8	55(2)	49(2)	49(2)	65(4)	6(3)
B	0.6240(8)	0.1240(8)	0	1.0	9(2)	–	–	–	–

[a] U_{eq} is defined as 1/3 of the trace of the orthogonalized U_{ij} tensors, $U_{13} = U_{23} = 0$, for boron (B) $U_{eq} = U_{iso}$ is the isotropic thermal parameter.

 © 2007 Wiley-VCH Verlag GmbH & Co. KGaA, Weinheim

3.02 Å, whereas the interchain distances are about 4.87 Å for the scandium atoms and about 6.60 Å for the iron atoms (Figure 1, bottom).

The interatomic distances in all three compounds are nearly the same, but those of the ruthenium-richer phase, $Sc_2FeRu_4RhB_2$, are in general a bit smaller as expected if compared with those of the rhodium-richer $Sc_2FeRu_2Rh_3B_2$ and $Sc_2FeRuRh_4B_2$ (see Table 3).

Table 3. Interatomic distances [Å] for $Sc_2FeRhRu_4B_2$, $Sc_2FeRh_3Ru_2B_2$ and $Sc_2FeRh_4RuB_2$. M′ replaces the atoms Ru and Rh sharing the same site (M′1 = Ru1/Rh1, M′2 = Ru2/Rh2).

			$Sc_2FeRu_4RhB_2$	$Sc_2FeRu_2Rh_3B_2$	$Sc_2FeRuRh_4B_2$
M′1	–M′1	1×	2.8214(9)	2.831(2)	2.809(2)
		2×	2.9827(6)	2.9933(9)	3.0144(8)
		2×	3.0117(5)	3.0192(6)	3.0187(6)
	–M′2	1×	2.7414(6)	2.7453(7)	2.7299(7)
	–Fe	2×	2.5915(4)	2.5997(5)	2.6118(5)
	–Sc	2×	2.831(1)	2.840(2)	2.840(2)
		2×	2.9306(6)	2.9357(9)	2.9307(8)
	–B	2×	2.184(3)	2.184(5)	2.178(4)
M′2	–M′1	4×	2.7414(6)	2.7453(7)	2.7299(7)
	–M′2	2×	3.0117(5)	3.0192(6)	3.0187(6)
	–Sc	4×	2.7513(8)	2.763(2)	2.765(1)
	–B	4×	2.223(5)	2.239(7)	2.229(6)
Fe	–M′1	8×	2.5915(4)	2.5997(5)	2.6118(5)
	–Fe	2×	3.0117(5)	3.0192(6)	3.0187(6)
Sc	–M′1	4×	2.831(1)	2.840(2)	2.840(2)
		4×	2.9306(6)	2.9357(9)	2.9307(8)
	–M′2	2×	2.7513(8)	2.763(2)	2.765(1)
	–Sc	2×	3.0117(5)	3.0192(6)	3.0187(6)
	–B	1×	2.655(6)	2.643(13)	2.654(8)
		2×	2.824(6)	2.844(9)	2.838(8)
B	–M′1	4×	2.184(3)	2.184(5)	2.178(4)
	–M′2	2×	2.223(5)	2.239(7)	2.229(6)
	–Sc	1×	2.655(6)	2.643(13)	2.654(8)
		2×	2.824(6)	2.844(9)	2.838(8)

The scandium intrachain distance of ≈3.02 Å, for each compound, is significantly shorter than the metallic separation for CN 12 (3.24 Å)[7] suggesting a size reduction due to charge transfer to the more electronegative B and M′ (Ru/Rh) atoms, in a first approximation. This trend was also found in other compounds of the $Ti_3Co_5B_2$-structure-type with distances varying from 3.03 to 3.17 Å.[3,4]

The iron intrachain distance (also ≈3.02 Å for each compound) is significantly longer than the iron metallic distance for CN 12 (2.52 Å)[7] but still short enough for bonding interactions to be considered, especially when it comes to the interpretation of the magnetic properties (see below). Nearly the same distances were obtained in all other compounds of the $Ti_3Co_5B_2$-type structure containing iron.[3,4]

The Sc–M′ (M′: Ru/Rh) distances ranging from 2.75 to 2.94 Å (average 2.84 Å) scatter between the average covalent radii sum of 2.75 Å (2.70 and 2.79 Å for Sc–Ru and Sc–Rh, respectively) and the average metallic radii sum for CN 12 of 2.95 Å (2.94 and 2.96 Å for Sc–Ru and Sc–Rh, respectively).[7] Comparable distances where found in $Sc_2Ru_5B_4$ (Sc–Ru distances vary from 2.63 to 3.14 Å)[8] and in $ScRh_3B$ (Sc–Rh distance is 2.88 Å).[9]

The M′–M′ distances (M′: Ru/Rh) vary from 2.73 to 3.02 Å with an average value of 2.89 Å, clearly wider than the metallic distance for CN 12 (2.67 and 2.68 Å for Ru–Ru and Rh–Rh, respectively)[7] but short enough for bonding interactions. Similar values were obtained in other transition-metal borides. In Ti_2Rh_6B (2.85 Å in BRh_6 octahedra),[10] in $Zn_{10}MRh_{18}B_8$ (average Rh–Rh = 2.89 Å with M: 3d element),[11] in $Sc_2Ru_5B_4$ (average Ru–Ru = 2.89 Å),[8] in $Sc_2MRh_5B_2$ (average Rh–Rh = 2.90 Å, with M: Cr, Mn, Fe).[4]

The average M′–B distance in each structure (≈2.20 Å) is the shortest one, and it is slightly wider than the average covalent radii sum of 2.07 Å (2.07 Å for either Ru–B or Rh–B); these interactions very probably correspond to the strongest bonds. Similar Ru–B and Rh–B bonds were found in the phases $Sc_2Ru_5B_4$ (2.18 Å),[8] $Ti_{1.6}Os_{1.4}RuB_2$ (2.16 Å),[12] $FeRh_6B_3$ (2.15 Å),[13] $Fe_xM'_{7-x}B_3$ (2.14 Å for M′: Ru and 2.13 Å for M′: Rh),[14] and $Sr_2Ru_7B_8$ (2.05–2.20 Å).[15]

Magnetism

In the following we will examine whether the new members of the $Sc_2FeRu_{5-n}Rh_nB_2$ series match the pattern of magnetic behavior given by the hitherto known representatives, and, for reasons of simplicity, we will start with the latter, then briefly mention the three new phases. Subsequently, all $Sc_2FeRu_{5-n}Rh_nB_2$-related results will be compared with the magnetic properties of those isoelectronic phases the VE counts of which have been adjusted by simultaneously replacing Sc by Mg, Fe by Mn, and Rh by Ir, as well as, by changing *n*. Curie paramagnetic contributions were solely attributed to the magnetic 3d atoms. The magnetically relevant parameters can all be found in Table 4.

***Antiferro- and ferromagnetism in $Sc_2FeRu_{5-n}Rh_nB_2$ phases* $Sc_2FeRu_{5-n}Rh_nB_2$; $n=0$ (60 VE), $n=2$ (62 VE), $n=5$ (65 VE)**: At high temperatures, the magnetic susceptibilities of the previously characterized[2a,5] intermetallics $Sc_2FeRu_5B_2$ (60 VE) and $Sc_2FeRu_3Rh_2B_2$ (62 VE) obey the Curie–Weiss

Table 4. Magnetic quantities for the compound series $Sc_2FeRu_{5-n}Rh_nB_2$ ($0 \le n \le 5$).

n	VE	AF, F[a]	T_N, T_C [K]	μ_a[b] [μ_B]	μ_{eff}[c] (400 K)	μ[d] [μ_B]	θ [K]	Range [K]	Ref.
0	60	AF	≈13(T_N)	–	2.1	3.9	−995	500–770	[2]
1	61	AF	≈10(T_N)	0.08	3.2	no Curie-Weiss behavior			this work
2	62	AF	–	–	3.6	4.0	−90	100–400	[6]
3	63	F	≈300(T_C)	3		4.2	375	500–800	this work
4	64	F	≈350(T_C)	3.1		no Curie-Weiss behavior			this work
5	65	F	≈450(T_C)	3.3		no Curie-Weiss behavior			[5]

[a] AF: Antiferromagnetism, F: Ferromagnetism. [b] μ_a: Atomic magnetic dipole moment at 4 K and $B_0 = 5$ T. [c] μ_{eff}: Effective Bohr magneton number; $\chi_m = \mu_0 \frac{N_A \mu_B^2}{3k_B T} \mu_{eff}^2$; $\mu_{eff} = 797.74 (\chi_m T)^{1/2}$ (SI units). [d] μ: Permanent paramagnetic moment calculated from the Curie constant *C*.

© 2007 Wiley-VCH Verlag GmbH & Co. KGaA, Weinheim

law $\chi_m = C/(T-\theta)$. The experimentally obtained Curie constants $C = 2.4\times10^{-5}$ and $2.5\times10^{-5}\,m^3\,K\,mol^{-1}$ correspond to paramagnetic moments $\mu = 3.9\,\mu_B$ and $4.0\,\mu_B$, respectively. The Weiss constants of $\theta = -995$ and -90 K indicate much stronger antiferromagnetic Fe–Fe interactions for the former. The intermetallic phase $Sc_2FeRh_5B_2$ ($n=5$ with 65 VE) orders ferromagnetically at $T_C = 450$ K, but above T_C Curie–Weiss behavior was not observed in the temperature range under investigation, thus, information for μ is lacking.[4] The atomic magnetic saturation moment μ_a^s per formula unit results in 3.3 μ_B at a temperature of 4 K and $B_0 = 5$ T. We now consider the new phases with intermediate VE counts (61, 63, and 64).

$Sc_2FeRu_4RhB_2$ (61 VE): Figure 2 exhibits the results of the magnetic susceptibility measurements at $4 \le T \le 800$ K and $0.01 \le B_0 \le 5$ T. The χ_m^{-1} versus T plot recorded at $B_0 = 2$ T

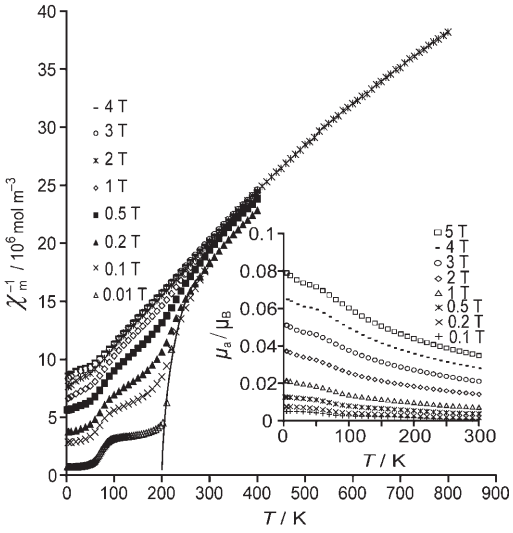

Figure 2. Reciprocal susceptibility versus temperature for $Sc_2FeRu_4RhB_2$ (61 VE) at various applied fields. The full line is just a guide for the eyes. Inset: Atomic magnetic dipole moment versus temperature at various applied fields.

deviates from a straight line. The overall high-temperature behavior, however, points to considerable antiferromagnetic Fe–Fe interactions. This finding becomes clear by comparing the μ_{eff} data (for definition see footnote [b] of Table 4), namely $\mu_{eff} = 2.1$, 3.2, and 3.6, at 400 K, for the systems with 60, 61, and 62 VE, respectively (see Table 4). In this series, the 61 VE compound takes up the intermediate position.

Upon varying the applied field in the range $0.01\ T \le B_0 \le 5$ T, at $T < 300$ K, one observes a characteristic field dependence of the magnetic susceptibility (see Figure 2):

a) χ_m decreases with increasing field until $B_0 = 1$ T is attained, and then it remains field-independent.
b) With decreasing temperature the field dependence of χ_m does increase up to one order of magnitude, but it yields only a small atomic magnetic dipole moment $\mu_a = 0.08\,\mu_B$ at 4 K and $B_0 = 5$ T (see insert of Figure 2).
c) At weak applied fields ($B_0 \le 0.1$ T) the typical behavior of a ferrimagnet is recognizable, sketched in Figure 2 by a solid line intersecting the T axis at the relatively high temperature of 200 K.
d) For $B_0 = 0.01$ T a broad maximum of the χ_m versus T plot is observed at around 10 K.

The complicated magnetic behavior of the compound with 61 VE may be the consequence of competing ferro- and antiferromagnetic interactions within and between the magnetic iron chains. It is worth mentioning that a similar behavior has also been observed for the 62 VE phase $Mg_2MnRh_5B_2$ below 50 K.[4] In order to get a deeper insight into the electronic situation of the two phases, further investigations are necessary, for example, neutron scattering experiments. First principles LMTO-ASA calculations, however, have already revealed antiferromagnetic Fe–Fe exchange interactions for the 61 VE phase with a complicated type of magnetic ordering, namely antiferromagnetism with incommensurate ordering vectors.[16]

$Sc_2FeRu_2Rh_3B_2$ (63 VE) and $Sc_2FeRuRh_4B_2$ (64 VE): Both phases are ferromagnets exhibiting spontaneous magnetization below $T_C = 300$ and 350 K respectively (T_C is deduced from the intersection of a linear fit of the steepest part of the magnetization curve with T at low applied fields[17]), and μ_a is 3.0 μ_B and 3.1 μ_B, respectively, at 4 K and $B_0 = 5$ T (see Figures 3 and 4). The paramagnetic region of the phase with

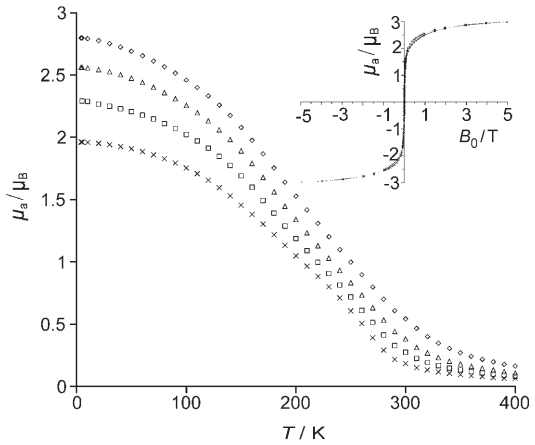

Figure 3. Magnetization versus temperature for $Sc_2FeRu_2Rh_3B_2$ (63 VE) at various applied fields; $B_0 = 2$ T (◇), 1 T (△), 0.5 T (□), and 0.2 T (×). Insert: Hysteresis loop at 4.5 K.

63 VE obeys the Curie–Weiss law at $T > 500$ K (see Figure 5) with $\theta \approx +375$ K and $C = 2.78\times10^{-5}\,m^3\,K\,mol^{-1}$, corresponding to $\mu = 4.2\,\mu_B$. For the 64 VE phase no Curie–Weiss behavior was observed in the paramagnetic range. With regard to the field dependence of μ_a, the two ferromagnets clearly differ (see inserts of Figures 3 and 4): Magnetic saturation was *not* achieved for the 63 VE compound even at 5 T, whereas the 64 VE phase already saturates mag-

 © 2007 Wiley-VCH Verlag GmbH & Co. KGaA, Weinheim

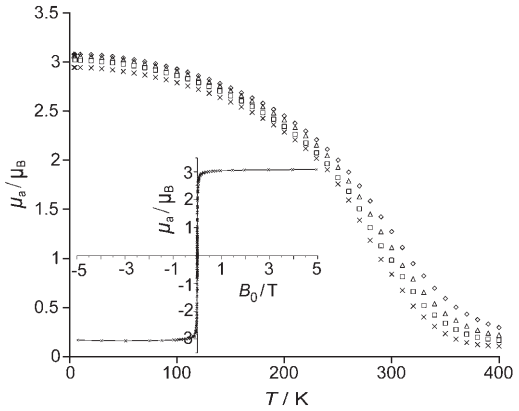

Figure 4. Magnetization versus temperature for $Sc_2FeRuRh_4B_2$ (64 VE) at various applied fields: $B_0 = 2$ T (◇), 1 T (△), 0.5 T (□), and 0.2 T (×). Insert: Hysteresis loop at 4.5 K.

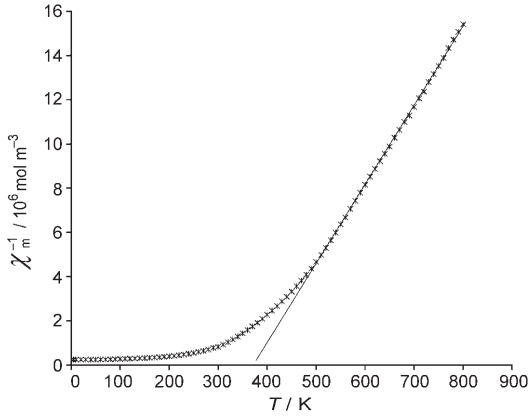

Figure 5. Reciprocal susceptibility versus temperature for $Sc_2FeRu_2Rh_3B_2$ (63 VE); Curie–Weiss behavior is observed ($B_0 = 5$ T). The straight line is just a guide for the eyes.

netically at 2 T. According to their hysteresis loops remanence and coercive field are very small, so that both intermetallics can be classified as soft ferromagnets such as $Sc_2FeRh_5B_2$ (65 VE).[2]

Trends in the $Sc_2FeRu_{5-n}Rh_nB_2$ series

The μ_{eff} versus T curves for the 60, 61, and 62 VE phases (Figure 6) clearly reveal a decrease of the antiferromagnetic exchange interactions as VE count increases; the incremental step is more pronounced from 60 to 61 VE than from 61 to 62 VE (see Table 4). This is also reproduced by the Weiss constant (θ): Although the 61 VE compound does not exactly follow the Curie–Weiss law, an estimate of θ (for comparison purposes) can be achieved by using two fictive straight lines where one matches the data between 400 and 600 K and the other between 600 and 800 K leading to θ values of about −200 and −400 K, respectively. Thus, the estimated θ range not only lies between the values obtained for the 60 and 62 VE phases as expected, but is also closer to −90 K (for the 62 VE phase) than to −995 K obtained for the 60 VE phase. In other words, the Fe–Fe antiferromagnetic interactions weaken in strength when the VE count increases from 60 to 62. The further increase of VE to 63 changes the Weiss constant dramatically from −90 to +375 K, thereby inducing a change of the nature of magnetic ordering and leading to a ferromagnet with a Curie temperature $T_C \approx 300$ K. Further increments of VE by one and two electrons strengthen the ferromagnetic behavior even more. For VE = 64 and 65, T_C increases to 350 and 450 K, as well as, μ_a to 3.1 μ_B and 3.3 μ_B, respectively. Hence, the Fe–Fe ferromagnetic interactions increase significantly between 63 and 65 VE with an increase of the number of valence electrons.

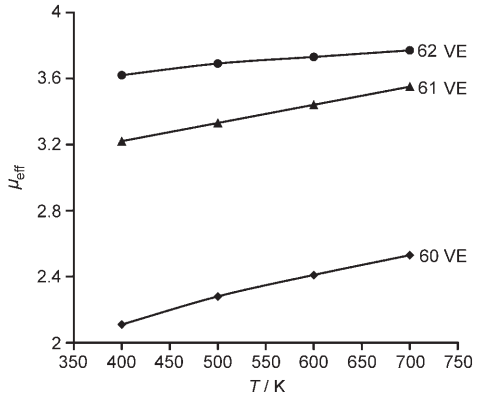

Figure 6. Effective magnetic moment versus temperature for $Sc_2FeRu_5B_2$ (60 VE), $Sc_2FeRu_4RhB_2$ (61 VE), and $Sc_2FeRu_3Rh_2B_2$ (62 VE).

To conclude, with an increasing VE count from 60 to 65 the series $Sc_2FeRu_{5-n}Rh_nB_2$ ($0 \le n \le 5$) exhibits a clear trend from antiferromagnetism to ferromagnetism. This result was correctly reproduced by first principles density-functional calculations of the ground-state magnetic ordering and exchange-interaction parameters[16] and it nicely corroborates the qualitative ideas at the very beginning of this research.[6]

Phases isoelectronic with $Sc_2FeRu_{5-n}Rh_nB_2$ ($0 \le n \le 5$)

In previous works, other isoelectronic phases with VE counts varying from 62 to 65 have been also studied. $Mg_2MnRh_5B_2$ (62 VE)[4,5] is, just like $Sc_2FeRu_3Rh_2B_2$ (62 VE), dominated by *antiferromagnetic* exchange interactions with Weiss constants $\theta = -130$ and −90 K, respectively. In contrast to $Sc_2FeRh_5B_2$ (65 VE) which is a ferromagnet, the isoelectronic $Sc_2FeIr_5B_2$ (65 VE),[3] however, was found to be a metamagnet, but nonetheless showing predominantly ferromagnetic coupling.

Theoretically, one could also expect metamagnetism for the intermediate phases with 63 and 64 VE, as they lie between the predicted antiferromagnets (62 VE) and ferromagnets (65 VE). Indeed, metamagnetism was observed in previous studies for $Mg_2FeRh_5B_2$ (63 VE) and $Sc_2MnRh_5B_2$ (64 VE),[4] both compounds exhibiting predominantly ferromagnetic coupling. Nonetheless, ferromagnetism has also

 © 2007 Wiley-VCH Verlag GmbH & Co. KGaA, Weinheim

been observed in $Sc_2MnIr_5B_2$ (64 VE, $T_C = +115$ K),[3] similar to the synthesized phases with 63 and 64 VE here. Generalizing, all compounds with 62 or less VE are governed by antiferromagnetic exchange interactions, whereas those with VE between 63 and 65 are either metamagnets or ferromagnets. It would also be interesting to further experimentally investigate the VE range above 65 VE: The series $Ti_2FeRu_{5-n}Rh_nB_2$ ($1 \le n \le 5$, 63 to 67 VE) is currently under investigation and will soon be communicated.

Conclusion

We have successfully synthesized and characterized, by combined single-crystal XRD analysis and EDX measurements, the new phases $Sc_2FeRu_4RhB_2$ (61 VE), $Sc_2FeRu_2Rh_3B_2$ (63 VE), and $Sc_2FeRuRh_4B_2$ (64 VE). All three crystallize in the $Ti_3Co_5B_2$ structure type with the magnetically active iron atom arranged in chains along the [001] direction and all are isostructural with their counterparts of the series $Sc_2FeRu_{5-n}Rh_nB_2$ ($0 \le n \le 5$). Magnetic measurements reveal ferromagnetism for phases with 63 and 64 VE and antiferromagnetism for the one with 61 VE, allowing the entire series $Sc_2FeRu_{5-n}Rh_nB_2$ ($0 \le n \le 5$) to exhibit a clear trend from antiferromagnetism (60 to 62 VE) to ferromagnetism (63 to 65 VE). Furthermore, as the VE count increases from 60 to 62 VE, the Fe–Fe antiferromagnetic interactions decrease significantly in strength, whereas, conversely, the Fe–Fe ferromagnetic interactions increase significantly by increasing the VE count from 63 to 65.

Experimental Section

Synthesis: Polycrystalline samples and single crystals of the series $Sc_2FeRu_{5-n}Rh_nB_2$ ($n = 1,3,4$) were synthesized by arc-melting the elements in water-cooled copper crucibles under an argon atmosphere by using a tungsten tip as a second electrode. The starting materials, scandium (pieces, 99.9%, Alfa Aesar), iron (powder, 99.9%, ABCR), rhodium (powder, 99.9%, Umicore), ruthenium (powder, 99.9%, Umicore), and boron (crystalline pieces, 99.999%, Alfa Aesar) were weighed in the respective atomic ratios, pressed into pellets and arc-melted under argon until homogeneous melting occurred; the argon was purified over silica gel, molecular sieves, and titanium sponge (950 K). The reaction products were remelted several times to ensure good homogeneity of the samples. Weight losses during the melting process were negligible. Silver-like products with metallic lustre were obtained with several single crystals suitable for X-ray structure analysis. The samples were all stable in air as compact bulk, as well as, fine-ground powders. The purity of the samples was checked by X-ray powder diffraction through Guinier powder diffractograms by using $Cu_{K\alpha 1}$ radiation ($\lambda = 1.54059$ Å) and silicon as an internal standard. The lattice parameters were refined on the basis of powder data with the program WinXPOW.[18] As it is almost impossible to differentiate rhodium and ruthenium by means of X-ray diffraction (they differ from each other by just one electron), the Ru:Rh ratio was quantitatively determined (see below) by Energy Dispersive X-ray analysis (EDX) on a high-resolution low-energy scanning electron microscope of the type LEO/Zeiss 1450 VP (Oberkochem, Germany) equipped with an EDX system of the type INCA (Oxford, England). The presence of the elements Sc and Fe and their ratios were also checked.

Structure determination: The lattice parameters obtained from powder data were used for the single-crystal structure refinements. Single crystals of suitable sizes were fixed on top of glass capillaries, and X-ray data were collected on a CCD single-crystal diffractometer (Bruker SMART APEX) with graphite-monochromatized $Mo_{K\alpha}$ radiation ($\lambda = 0.71073$ Å). The X-ray intensities were corrected with respect to absorption by using a semiempirical procedure.[19] The crystal structures were refined by full-matrix least-squares refinement,[20] based on F^2, by using anisotropic displacement parameters for Sc, Fe, and Ru/Rh and an isotropic one for B. EDX measurements on several selected crystals provided the same Fe/Sc ratio (1:2.09, averaged experimental data) for all compounds, and analytical Ru:Rh ratios of 4.04:1, 2:3.06, and 1:4.03 (averaged experimental data) were obtained for $Sc_2FeRu_4RhB_2$, $Sc_2FeRu_2Rh_3B_2$, and $Sc_2FeRuRh_4B_2$, respectively, in very good agreement with the ideal ratios calculated from the respective chemical formula. As $Sc_2FeRh_5B_2$[2,4,5] is isotypic with the investigated compounds, its structure was used as starting model for the structure refinement. By using the above-mentioned starting model all refinements converged with very good internal R values. Replacing rhodium by ruthenium in the structure did not influence the refinement because nearly the same internal R values where obtained. Therefore the rhodium/ruthenium ratio obtained from the EDX analyses (which also agree with the expected values, reflected by single-phase powder diffractograms) were imposed to the structure model (see Table 2) for the final proper refinements. The atomic positions for all data were then standardized with the program STRUCTURE TIDY.[21] All relevant crystallographic data and experimental details of the data collection are listed in Table 1. Table 2 contains the atomic coordinates and displacement parameters, whereas the interatomic distances are listed in Table 3. Drawings were performed by using the program Diamond.[22] Further details on the crystal structure investigation may be obtained from the Fachinformationszentrum Karlsruhe, 76344 Eggenstein-Leopoldshafen, Germany (fax: (+49) 7247-808-666; e-mail: crysdata@fiz-karlsruhe.de), on quoting the depository numbers CSD-417587 for $Sc_2FeRu_4RhB_2$, -417588 for $Sc_2FeRu_2Rh_3B_2$, and 417586 for $Sc_2FeRuRh_4B_2$.

Magnetization measurements: The measurements of magnetic properties were carried out on polycrystalline samples (mainly selected crystals, weighed portions 2–9 mg) by using a SQUID magnetometer (MPMS-5S, Quantum Design, San Diego, USA; temperature range $4 \le T \le 800$ K, applied field up to 5 T). The samples were collected by manual selection of larger crystals under an optical microscope. These were then coarsely ground and encapsulated in quartz tubes. Details concerning sample arrangement and measurement techniques are described elsewhere.[2b,23] Corrections for diamagnetic and conduction electron contributions were not applied. Demagnetization corrections were applied for the hystereses data.

Acknowledgement

The authors thank Deutsche Forschungsgemeinschaft for financial support (DFG fellowship to B.F.), Klaus Kruse, and Dipl. Chem. Manfred Speldrich for measurement of the magnetic data, Ramona Gruel for experimental help, Dr. Roland Winde (Umicore, Hanau–Wolfgang) for the kind donation of ruthenium and rhodium metals, and Resi Zaunbrecher (IPC, RWTH Aachen) for the EDX analyses.

[1] Yu. B. Kuz'ma, Y. P. Yarmolyuk, *Zh. Strukt. Khim.* **1971**, *12*, 458.
[2] a) E. A. Nagelschmitz, Dissertation, University of Cologne, Cologne (Germany) **1995**; b) R. Feiten, Dissertation, RWTH Aachen University, Aachen (Germany) **1996**.
[3] E. A. Nagelschmitz, W. Jung, *Chem. Mater.* **1998**, *10*, 3189.
[4] E. A. Nagelschmitz, W. Jung, R. Feiten, P. Müller, H. Lueken, *Z. Anorg. Allg. Chem.* **2001**, *627*, 523.
[5] R. Dronskowski, K. Korczak, H. Lueken, W. Jung, *Angew. Chem.* **2002**, *114*, 2638; *Angew. Chem. Int. Ed.* **2002**, *41*, 2528.

 © 2007 Wiley-VCH Verlag GmbH & Co. KGaA, Weinheim

[6] a) G. A. Landrum, R. Dronskowski, *Angew. Chem.* **2000**, *112*, 1598; *Angew. Chem. Int. Ed.* **2000**, *39*, 1560; b) R. Dronskowski, *Computational Chemistry of Solid State Materials*, Wiley-VCH, Weinheim, **2005**.
[7] L. Pauling, *J. Am. Chem. Soc.* **1947**, *69*, 542.
[8] P. Rogl, *J. Solid State Chem.* **1984**, *55*, 262.
[9] U. Berger, W. Schnick, *J. Alloys Compd.* **1994**, *206*, 179.
[10] B. P. T. Fokwa, B. Eck, R. Dronskowski, *Z. Kristallogr.* **2006**, *221*, 445.
[11] U. Eibenstein, W. Jung, *Z. Anorg. Allg. Chem.* **1998**, *624*, 802.
[12] B. P. T. Fokwa, J. von Appen, R. Dronskowski, *Chem. Commun.* **2006**, 4419.
[13] B. P. T. Fokwa, R. Dronskowski, *Z. Anorg. Allg. Chem.* **2005**, *631*, 2478.
[14] B. P. T. Fokwa, R. Dronskowski, *J. Alloys Compd.* **2007**, *428*, 84.
[15] W. Jung, F. Diessenbacher, *Z. Anorg. Allg. Chem.* **1991**, *594*, 57.
[16] G. Samolyuk, B. P. T. Fokwa, R. Dronskowski, G. J. Miller, unpublished results.
[17] R. Andrés, M. Brissard, M. Gruselle, C. Train, J. Vaissermann, B. Malézieux, J.-P. Jamet, M. Verdaguer, *Inorg. Chem.* **2001**, *40*, 4633.
[18] WinXPOW, Version 1.06, STOE Cie., Darmstadt, **1999**.
[19] G. M. Sheldrick, SADABS, University of Göttingen, Göttingen (Germany), **2001**.
[20] G. M. Sheldrick, SHELXL-97, Program for the refinement of crystal structures, University of Göttingen, Göttingen (Germany), **1997**.
[21] L. M. Gelato, E. Parthé, *J. Appl. Crystallogr.* **1987**, *20*, 139.
[22] K. Brandenburg, DIAMOND, Visual Crystal Information System, Bonn, **1999**.
[23] H. Lueken, *Magnetochemie*, Teubner, Stuttgart, **1999**.

Received: January 24, 2007
Published online: April 30, 2007

 © 2007 Wiley-VCH Verlag GmbH & Co. KGaA, Weinheim